nature biotechnology

LETTERS

Bright and stable near-infrared fluorescent protein for *in vivo* imaging

Grigory S Filonov[1], Kiryl D Piatkevich[1], Li-Min Ting[2], Jinghang Zhang[3], Kami Kim[2] & Vladislav V Verkhusha[1]

Imaging biological processes in mammalian tissues will be facilitated by fluorescent probes with excitation and emission bands within the near-infrared optical window of high transparency[1]. Here we report a phytochrome-based near-infrared fluorescent protein (iRFP) with excitation and emission maxima at 690 nm and 713 nm, respectively. iRFP does not require an exogenous supply of the chromophore biliverdin and has higher effective brightness, intracellular stability and photostability than earlier phytochrome-derived fluorescent probes. Compared with far-red GFP-like proteins, iRFP has a substantially higher signal-to-background ratio in a mouse model due to its infrared-shifted spectra.

Molecular imaging using fluorescent proteins is an important technique to quantitatively and noninvasively monitor biological processes ranging from gene expression to angiogenesis, from tumor growth and metastasis to bacterial and viral infections[2]. In mammals, deep tissue visualization of the conventional fluorescent proteins derived from the green fluorescent protein family (GFP-like fluorescent proteins) is hindered by the high absorbance of hemoglobin and skin melanin. An optimal fluorescent protein for *in vivo* imaging should have both excitation and emission maxima within a near-infrared window from ~650 nm to 900 nm, for which tissue has the lowest absorbance[1] and less light scattering than in the shorter wavelength part of the spectrum[3]. However, to this date even the most far-red-shifted GFP-like proteins still have excitation spectra outside of the near-infrared window.

Alternatively, near-infrared fluorescent proteins can be engineered on the basis of phytochromes[4]. Phytochromes are photosensory receptors that absorb light in the red and far-red part of spectrum[5]. The family of phytochromes shares a conserved photosensory protein core consisting of a PAS domain, a GAF domain and a PHY domain. A linear tetrapyrrole chromophore, such as biliverdin IXα (BV), phycocyanobilin or phytochromobilin, is covalently bound to either the PAS or the GAF domain. Bacteriophytochromes are good candidates for design templates for near-infrared fluorescent proteins, because BV, the obligatory co-factor of bacteriophytochromes, is an intermediate of the normal mammalian heme metabolism[6].

The fluorescent properties of phytochromes have been known for a long time[4,7–9] but only recently a near-infrared fluorescent mutant of the *Dr*BphP bacteriophytochrome from *Deinococcus radiodurans*, named IFP1.4, was reported to be useful for *in vivo* imaging[10]. However the properties of IFP1.4, such as *in vitro* and *in vivo* effective brightness and photostability, remain suboptimal and require development of new superior probes.

To engineer an improved near-infrared fluorescent protein, we turned to another template—bacteriophytochrome *Rp*BphP2 (ref. 11) from the photosynthetic bacterium *Rhodopseudomonas palustris*. The full-length *Rp*BphP2 protein is weakly fluorescent at 725 nm when excited at 710 nm[11].

First, we truncated *Rp*BphP2 and retained only the PAS and GAF domains (*Rp*BphP2-PAS-GAF; 316 amino acids in length). We also introduced a D202H mutation, because substitutions of this aspartic acid have been shown to improve the fluorescent properties of the phytochromes[9,12]. Bacteria expressing this *Rp*BphP2-PAS-GAF/D202H variant and a heme-oxygenase (to produce the BV co-factor) were weakly fluorescent.

The *Rp*BphP2-PAS-GAF/D202H variant was then subjected to three rounds of random mutagenesis followed by a round of saturating mutagenesis of the identified key residues. The brightest clones in each library were isolated using fluorescence-activated cell sorting (FACS) and then used as a template for the next round of mutagenesis. The final mutant had the following 13 substitutions: S13L, A92T, V104I, V114I, E161K, Y193K, F198Y, D202T, I203V, Y258F, A283V, K288T and N290Y (**Supplementary Fig. 1**). This variant was named iRFP (infrared fluorescent protein).

Compared to IFP1.4, iRFP exhibited a higher extinction coefficient (**Fig. 1a** and **Table 1**) as determined by direct measurement of the protein concentrations. Extinction coefficients calculated as suggested in reference[10] (based on the comparison of the proteins' main absorbance peaks with their peaks at 391 nm, which correspond to the absorbance of BV) were similar. iRFP fluorescence exhibited excitation and emission maxima at 690 nm and 713 nm, respectively (**Fig. 1b**), slightly red-shifted compared to IFP1.4. Quantum yields at pH 7.5 measured 5.9% for iRFP and 7.7% for IFP1.4. Based on these measurements the molecular brightness of iRFP is 20% higher than that of IFP1.4 (**Table 1**).

iRFP had a slightly slower maturation rate at 37 °C than IFP1.4 with a maturation half-time of 2.8 h versus 1.9 h for IFP1.4 (**Fig. 1c** and **Table 1**). The fluorescence of iRFP was pH stable with a pK_a value of 4.0, compared to a pK_a of 4.6 for IFP1.4 (**Fig. 1d** and **Table 1**).

Size-exclusion chromatography demonstrated that iRFP was a dimer whereas IFP1.4 contained two fractions: a monomer, and oligomers with an apparent MW of ~190 kDa (**Supplementary Fig. 2**).

[1]Department of Anatomy and Structural Biology and Gruss-Lipper Biophotonics Center, Albert Einstein College of Medicine, Bronx, New York, USA. [2]Department of Medicine and Department of Microbiology and Immunology, Albert Einstein College of Medicine, Bronx, New York, USA. [3]Flow Cytometry Core Facility, Albert Einstein College of Medicine, Bronx, New York, USA. Correspondence should be addressed to V.V.V. (vladislav.verkhusha@einstein.yu.edu).

Received 28 February; accepted 15 June; published online 17 July 2011; doi:10.1038/nbt.1918

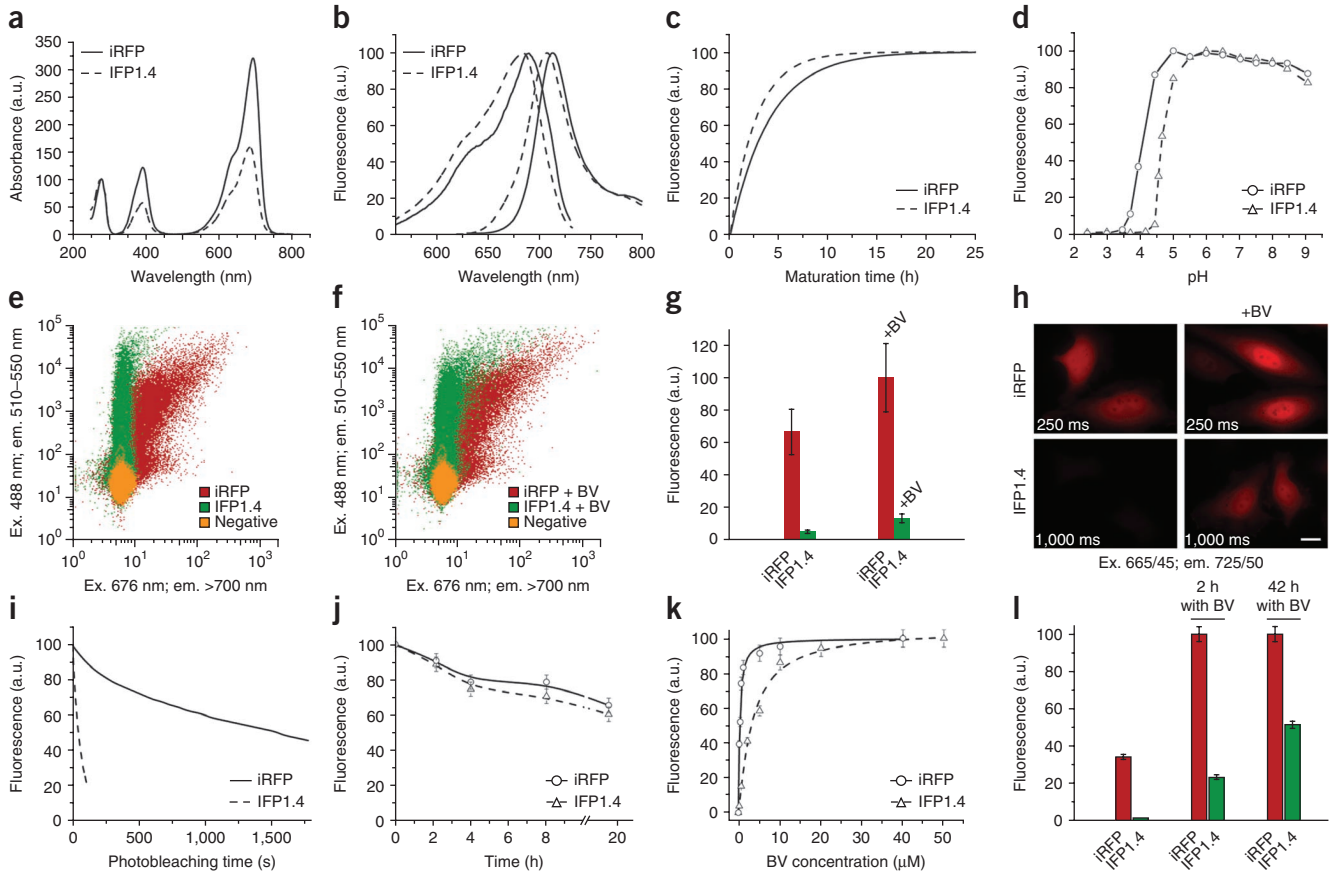

Figure 1 *In vitro* properties of iRFP and IFP1.4. (**a**) Absorbance in arbitrary units (a.u.) with absorbance at 280 nm set to 100%. (**b**) Fluorescence excitation and emission spectra normalized to 100% for both proteins. (**c**) Fitted curves of the maturation kinetics in hours in bacteria at 37 °C. (**d**) Equilibrium pH dependence of fluorescence. (**e**,**f**) FACS dot-plots representing near-infrared fluorescence of iRFP and IFP1.4 (*x* axis) and green fluorescence from co-expressed EGFP (*y* axis) of transiently transfected HeLa cells not treated (**e**) or treated (**f**) with 25 μM of BV for 2 h before analysis. A 676 nm laser line for excitation (ex.) and a 700 nm long pass filter to collect emission (em.) from iRFP and IFP1.4 were used. (**g**) Mean near-infrared fluorescence intensity of the double-positive cells from **a** and **b** normalized to transfection efficiency (EGFP signal), absorbance of the respective protein at 676 nm and overlap of the fluorescence spectrum of the respective protein with the transmission of the emission filter. (**h**) Fluorescent images of the transiently transfected HeLa cells with and without addition of 25 μM BV for 2 h before imaging. Scale bar, 20 μm. (**i**) Photobleaching in HeLa cells. The curves were normalized to absorbance spectra and extinction coefficients of the proteins (calculated based on BV absorbance), spectrum of an arc lamp and transmission of a photobleaching filter. Plot represents the data obtained with endogenous BV but both proteins demonstrated no change in photostability after addition of exogenous BV. (**j**) Degradation of the proteins in HEK293 cells after treatment with 1 mM puromycin. Cells were incubated with 25 μM BV to achieve a higher fluorescent signal. Protein concentration was assessed by measuring fluorescence intensity of crude cell lysates. (**k**) BV binding to iRFP and IFP1.4 proteins in HeLa cells. Cells were incubated with the respective amounts of BV for 2 h before harvesting on the second day after adenovirus infection. Fluorescence intensity was measured in crude cell lysates and normalized to 100%. Lines are fitted based on the Scatchard equation. (**l**) Protein expression in HeLa cells 48 h after adenovirus infection. Data for the cells without exogenous BV, with 25 μM of BV added 2 h and 42 h before the analysis are shown. Fluorescence intensities were normalized to the total cell number, excitation wavelength, emission collection bandwidth and protein molecular brightness to represent the iRFP or IFP1.4 concentrations.

The IFP1.4 oligomers may also exist in mammalian cells, potentially limiting the utility of IFP1.4 as a fusion tag. By contrast, iRFP exhibited a clear dominant dimer peak. Tandem engineering strategies[13] may allow iRFP to be developed as a fusion tag.

Quasi-equilibrium curves of protein unfolding, induced by guanidinium chloride (GndCl)[14], demonstrated that iRFP has a higher conformation stability than IFP1.4 (**Table 1** and **Supplementary Fig. 3a**). The calculated difference in free energies of unfolding[15,16] between the iRFP and IFP1.4 proteins was 3.5 kcal/mole. Because iRFP and IFP1.4, like other phytochromes[6], bind BV covalently (**Supplementary Fig. 4**), the GndCl-induced decrease in fluorescence indicates the loss of the proteins' tertiary structures rather than BV dissociation, indicating that iRFP is substantially more thermodynamically stable.

The normalized photostability of iRFP, as measured in aqueous drops in oil, was about tenfold higher than that of IFP1.4 (**Supplementary Fig. 3b** and **Table 1**). To exclude the possibility that the experiments revealed residual intrinsic photoswitching properties of phytochromes instead of measuring bleaching, the aqueous drops were left in the dark for an additional 30 min after irradiation with photobleaching light and were then imaged again (**Supplementary Fig. 3b**). Neither protein showed any increase in fluorescence, suggesting that both remained in the main, non-photoswitched state and that the observed loss of fluorescence was caused by photobleaching.

The two-photon excitation spectrum of purified iRFP measured in the 1,100–1,340 nm spectral region revealed an excitation peak at 1,260 nm corresponding to the main one-photon absorbance

Table 1 ***In vitro*** **properties of iRFP in comparison with IFP1.4**

Protein	Absorbance maximum (nm)	Excitation maximum (nm)	Emission maximum (nm)	Extinction coefficient ($M^{-1}cm^{-1}$) (based on protein concentration)	Extinction coefficient ($M^{-1}cm^{-1}$) (calculated based on BV absorbance)	Quantum yield (%)	Molecular brightness relative to IFP1.4 (%)	Photostability, $\tau_{50\%}$ (s)	p*Ka*	Maturation at 37 °C, 50% (h)	Conformational stability in GndCl, $[D]_{50\%}$ (M)
iRFP	692	690	713	85,000	105,000	5.9	120	450	4.0	2.8	2.9
IFP1.4	684	684 (684)	707 (708)	54,700	102,000 (92,000)	7.7 (7.0)	100	50	4.6	1.9	1.7

IFP1.4 characteristics from the original paper[10] are shown in parentheses. Spectroscopic parameters were determined in PBS at pH 7.5.

maximum (**Supplementary Fig. 5**). Thus iRFP is also suitable for multiphoton imaging, though its two-photon properties need to be studied further.

To characterize iRFP in mammalian cells, we used FACS to analyze HeLa cells transiently transfected with iRFP- and IFP1.4-encoding plasmids (no exogenous heme-oxygenase gene was used here). Cells were co-transfected with an EGFP plasmid for near-infrared signal normalization. As the amount of endogenous BV might not be enough to bind all apoproteins, where indicated, a saturating concentration[10] of 25 µM BV was added to the culture medium 2 h before analysis.

Despite the slight differences in molecular brightness of the phytochromes, the fluorescence signals of the iRFP- and IFP1.4-expressing cells differed drastically (**Fig. 1e**,**f**). Whereas the iRFP cells showed bright fluorescence even without addition of exogenous BV, the IFP1.4 fluorescence was observed only in the cells expressing EGFP (and thus phytochromes) at high levels and in the presence of exogenous BV. Quantification of this difference, performed by normalizing phytochrome signal to EGFP signal, showed that iRFP cells were 13-fold brighter than the IFP1.4 cells without exogenous BV and sevenfold brighter after addition of BV (**Fig. 1g** and **Supplementary Table 1**). Therefore the effective brightness of iRFP in living cells, which is a combination of molecular brightness, intracellular stability, affinity for BV and protein expression level, is substantially higher than that of IFP1.4. To compare the relative concentrations of the produced fluorescent molecules of iRFP and IFP1.4, the normalized cellular fluorescence intensities were divided by the respective molecular brightness. The cellular amount of the iRFP fluorescent molecules was 5.9-fold and 11.0-fold greater than that of IFP1.4 with and without exogenous BV, respectively (**Supplementary Table 1**).

Epifluorescent microscopy of the transiently transfected HeLa cells showed evenly dispersed fluorescent signals without any intracellular aggregates for both proteins (**Fig. 1h**). Addition of exogenous BV and fourfold longer exposure times were typically required to obtain images of the IFP1.4 cells of the same brightness as images of the iRFP cells without exogenous BV. The normalized intracellular photostability of iRFP was even higher than in aqueous drops whereas the photostability of IFP1.4 was similar, with an overall ~30-fold difference between the two proteins (**Fig. 1i** and **Supplementary Table 1**).

To assess the degradation kinetics of iRFP and IFP1.4, cells expressing one of the proteins were treated with 1 mM puromycin to inhibit protein translation[17]. The fluorescence of both proteins was stable in cells and exhibited similar degradation time-courses over a period of 20 h (**Fig. 1j**).

As the brightness of the IFP1.4-expressing cells increased more upon BV addition than that of iRFP-expressing cells (**Fig. 1g**), we studied whether the proteins had different BV binding efficiencies. Different BV concentrations were added to HeLa cells expressing either IFP1.4 or iRFP, and the BV-binding curves (**Fig. 1k**) were fitted and processed using a Scatchard equation[18]. The BV dissociation constants for iRFP and IFP1.4 were 0.35 µM and 4.2 µM, respectively (**Supplementary Table 1**). The data suggest that the 12-fold higher iRFP binding affinity allows efficient formation of iRFP-BV fluorescent complexes despite the relatively low concentrations of endogenous BV in cells.

To assess the intracellular stability of the iRFP and IFP1.4 apoproteins, we expressed iRFP and IFP1.4 in HeLa cells without or with exogenous BV added for short (2 h) or long (42 h) periods of time before the assay. Expression of IFP1.4 in the presence of BV for 42 h resulted in cells that were twice as fluorescent as cells maintained with BV for 2 h. In contrast, prolonged BV exposure had no effect on iRFP fluorescence (**Fig. 1l** and **Supplementary Table 1**). Similar results were obtained by expressing the proteins in bacteria bearing the heme-oxygenase without and with added heme precursors (**Supplementary Fig. 6**). Overall, these data suggested that BV binding to the IFP1.4 apoprotein was required to stabilize it, possibly by preventing intracellular degradation. By contrast, the majority of the iRFP apoprotein molecules remained intact for at least 2 d as suggested by the similar brightness of the iRFP cells exposed to exogenous BV for short and long time periods (**Fig. 1l**).

To study the toxicity of the proteins in mammalian cells, we used an approach that has previously been employed for GFP-like proteins[19]. iRFP, IFP1.4 and control GFP/S65T variant were transiently expressed for 1, 3 and 5 d in HeLa cells and the mean fluorescence intensity of the viable cells was determined by FACS (**Supplementary Fig. 7**). If the fluorescent proteins were cytotoxic then the fluorescence intensity of the expressing cells would rapidly decrease[19]. In agreement with the previous data[20,21], the GFP-producing cells demonstrated a bell-shaped profile of the expression. By contrast, the apparent expression of iRFP and IFP1.4 steadily increased for 5 d. We attributed this increase to a combination of two processes: the high-level production of exogenous apoproteins and a 'catching up' synthesis of endogenous BV to bind it, thus forming the fluorescent holoproteins. However, these proteins' behavior precluded us from the assessment of the cytotoxicity in this essay.

These results prompted us to look for longer expression conditions where the holoprotein level could remain constant. For this purpose preclonal mixtures of HeLa cells expressing iRFP, E2-Crimson (noncytotoxic standard)[22] or mKate2 (cytotoxic standard)[22] were made. Prolonged expression of IFP1.4 at detectable levels required constant BV addition that might affect the results; therefore, it was not assessed in this assay. Cells with iRFP, E2-Crimson or mKate2 were maintained for 21 d after the transfection with a selection drug, sorted and finally analyzed after 20 more days in selection medium. E2-Crimson- and iRFP-sorted cell populations remained mostly within the original sorting gates whereas the majority of the sorted mKate2 cells lost their fluorescence (**Supplementary Fig. 8**). Because iRFP-expressing cells behaved similarly to the cells expressing noncytotoxic control E2-Crimson we concluded that iRFP was not cytotoxic.

Next, iRFP applicability for imaging in mammals was tested. Mice were infected with adenoviral particles containing a gene encoding either iRFP or IFP1.4 and then imaged using an IVIS Spectrum imager. Fluorescence of the liver in the iRFP-infected mice was

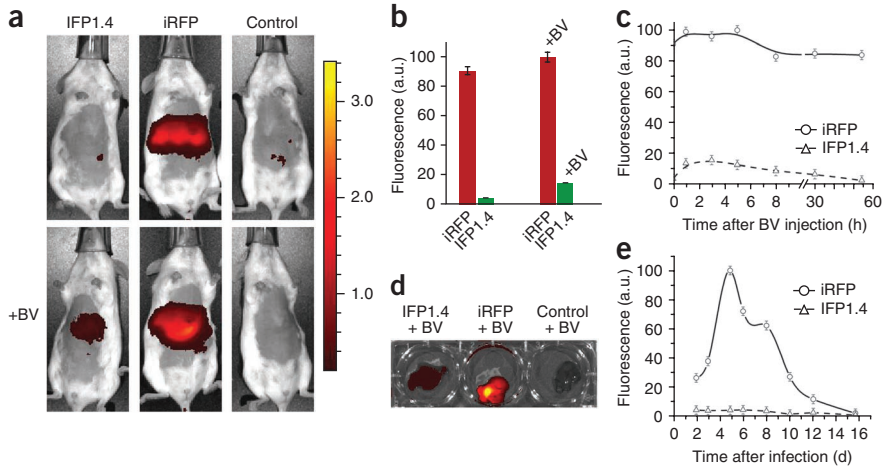

Figure 2 Expression of iRFP in living mouse. (**a**) Overlay of representative light and fluorescent images of iRFP or IFP1.4 adenovirus infected mice with and without injection of 250 nmol BV. A non-infected control mouse is shown on the right. The fluorescence images were acquired using IVIS Spectrum instrument equipped with 675/30 nm excitation and 720/20 nm emission filters. The color bar indicates the fluorescence radiant efficiency, multiplied by 10^9. (**b**) Near infrared fluorescence total radiant efficiency of the liver areas of the iRFP and IFP1.4 expressing mice in (**a**), normalized to the bandwidth of the excitation and emission filters. (**c**) Time course of the near-infrared fluorescence total radiant efficiency of the liver areas of the iRFP and IFP1.4 expressing mice in (**a**) after BV injection. (**d**) Overlay of the photograph and fluorescent image of the isolated livers from the BV-injected infected and non-infected (control) mice. (**e**) Time course of the near-infrared fluorescence total radiant efficiency of the liver areas of the mice not being injected with BV. The fluorescence signals in **c** and **e** were also normalized to the bandwidth of the excitation and emission filters.

detected starting the second day after infection, with the peak intensity at day 5 (**Fig. 2a**). The IFP1.4-expressing mice showed weak liver fluorescence throughout the experiment. At day 5 after infection 250 nmol of BV was administered to both experimental groups of mice. After the injection, the IFP1.4-infected livers became about fourfold brighter; however, they still were dimmer than the iRFP-expressing livers. Calculation of total radiant efficiencies of the liver regions demonstrated the iRFP effective brightness *in vivo* being 22-fold higher without exogenous BV and sevenfold higher after BV injection (**Fig. 2b**).

Following BV administration, the IFP1.4 liver fluorescence lost half of its brightness after ~30 h and returned to the initial brightness ~2 d after the injection (**Fig. 2c**). The decrease in brightness of the iRFP liver during the 2-d period after the BV injection was only ~10%. These data suggest that in contrast to iRFP, prolonged mouse experiments involving IFP1.4 will require frequent BV injections.

Correct localization of both proteins was revealed by *ex vivo* imaging of the isolated livers (**Fig. 2d**). The iRFP fluorescence was easily detected in the liver 10 d after infection without administrating BV during this period (**Fig. 2e**), suggesting that iRFP is both stable and noncytotoxic *in vivo*. iRFP expression in other than liver tissues with no need for exogenous BV was demonstrated by *ex vivo* imaging of the spleen excised from an infected mouse (**Supplementary Fig. 9**).

To provide additional support for the general applicability of iRFP for different body tissues, the fluorescence of liver cells isolated from iRFP-infected and control mice was compared to the fluorescence of stably iRFP-expressing cultured cells that originated from human cervix, rat brain and rat mammary gland. The cultured cells showed a similar or higher brightness than mouse hepatocytes without adding exogenous BV (**Supplementary Fig. 10**), suggesting that iRFP is suitable for imaging of various organs and tissues.

A molecular evolution approach enabled us to develop an advanced near-infrared fluorescent protein with excitation and emission maxima inside of the near-infrared window. We expect that this genetically encoded iRFP probe will be a valuable tool for *in vivo* studies in small mammals.

In many respects, the properties of iRFP are superior to those of IFP1.4. First, iRFP has a higher molecular brightness and greater photostability. Second, iRFP exhibits greater thermodynamic stability, a lower pK_a value and a higher binding affinity to BV. Third, iRFP has much higher effective brightness in cells and in mice, as the IFP1.4 apoprotein has a lower affinity to BV and is not stable without it. Lastly, iRFP does not require

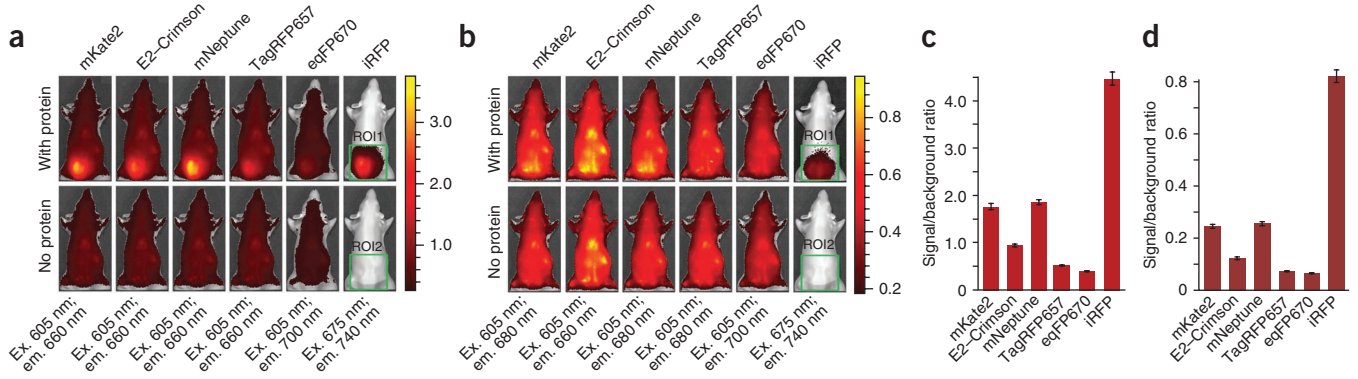

Figure 3 Comparison of iRFP with far-red GFP-like proteins in mouse phantom. (**a**,**b**) Samples consisting of equal amounts of the purified proteins of the same concentration were placed inside of the phantom mouse in bores located 7.0 mm (**a**) or 18.1 mm (**b**) deep from the mouse surface. Each protein sample was imaged using epifluorescence mode in several wavelength channels. A signal-to-background ratio in each channel was calculated as (ROI1 - ROI2) / ROI2, where ROI1 or ROI2 were total radiant efficiencies of the respective areas with and without the protein sample. Images for the highest signal-to-background ratio for each protein are shown. The color bar indicates the fluorescence radiant efficiency, multiplied by 10^8. (**c**,**d**) The highest signal-to-background ratio values, calculated for the respective images in **a** and **b**.

addition of an external BV when imaged in mammalian cells or in mice, and in this respect it behaves similarly to GFP-like proteins.

Several GFP-like far-red fluorescent proteins have been shown to be useful for whole-body imaging[23,24], however, their spectral properties are suboptimal for this purpose. To directly compare iRFP deep-tissue imaging performance with that of far-red-shifted fluorescent proteins, such as mKate2 (ref. 25), E2-Crimson[22], mNeptune[23], TagRFP657 (ref. 26) and eqFP670 (ref. 24), we imaged the same amount of purified proteins at 7.0 and 18.1 mm depth inside of a mouse phantom, which has the autofluorescence and light-scattering properties matching those of mouse muscle tissue[27,28] (**Fig. 3a**,**b**). To compare brightness in different spectral channels, the signal-to-background ratio for the fluorescent proteins was calculated for each channel. The highest ratio values among the different channels are shown (**Fig. 3c**,**d**). iRFP has 2.4-fold and 3.2-fold larger ratio values at 7.0 mm and 18.1 mm depth, respectively, than the best in this experiment GFP-like fluorescent protein mNeptune. The data confirmed that the far-red-shifted spectrum allows iRFP to perform substantially better despite being less bright on the molecular level.

In conclusion, to our knowledge, iRFP is currently, both in terms of molecular and effective brightness, the brightest phytochrome-based and the fluorescent protein whose spectrum is shifted most to the infrared. iRFP is stable, noncytotoxic and the low concentrations of endogenous BV are sufficient to make it brightly fluorescent in cells, tissues and whole animals. These features make its application as easy as the conventional GFP-like fluorescent proteins and hence should broaden the possibilities of noninvasive *in vivo* imaging.

METHODS

Methods and any associated references are available in the online version of the paper at http://www.nature.com/naturebiotechnology/.

Note: Supplementary information is available on the Nature Biotechnology website.

ACKNOWLEDGMENTS

We thank E. Giraud (Institute for Research and Development, France) for the plasmid encoding bacteriophytochrome from *R. palustris*, A. Ulijasz and R. Vierstra (both from University of Wisconsin) for the plasmid encoding the heme-oxygenase from *Synechocystis* sp. PCC6803 and B. Glick (University of Chicago), D. Chudakov and K. Lukyanov (both from Institute of Bioorganic Chemistry, Russia) for the plasmids encoding GFP-like far-red fluorescent proteins. We are grateful to D. Entenberg for the help with two-photon excitation measurements, A. Muesch and D. Cohen for the assistance with virus purification and providing GFP-encoding adenoviruses and R. Zheng for the help with size-exclusion chromatography (all from Albert Einstein College of Medicine). This work was supported by grants from the US National Institutes of Health, AI046985 and AI087625 to K.K., GM073913 to V.V.V. and S10RR027308 for purchase of the IVIS imager.

AUTHOR CONTRIBUTIONS

G.S.F. developed the protein and together with K.D.P. characterized it *in vitro*. G.S.F. studied the protein in mammalian cells. G.S.F. and J.Z. analyzed and sorted cells using FACS. G.S.F., L.-M.T. and K.K. characterized protein expression in mice. V.V.V. designed and planned the project and together with G.S.F. wrote the manuscript.

COMPETING FINANCIAL INTERESTS

The authors declare no competing financial interests.

Published online at http://www.nature.com/nbt/index.html.
Reprints and permissions information is available online at http://www.nature.com/reprints/index.html.

1. Jobsis, F.F. Noninvasive, infrared monitoring of cerebral and myocardial oxygen sufficiency and circulatory parameters. *Science* **198**, 1264–1267 (1977).
2. Hoffman, R.M. The multiple uses of fluorescent proteins to visualize cancer *in vivo*. *Nat. Rev. Cancer* **5**, 796–806 (2005).
3. Ntziachristos, V. Going deeper than microscopy: the optical imaging frontier in biology. *Nat. Methods* **7**, 603–614 (2010).
4. Fischer, A.J. & Lagarias, J.C. Harnessing phytochrome's glowing potential. *Proc. Natl. Acad. Sci. USA* **101**, 17334–17339 (2004).
5. Sharrock, R.A. The phytochrome red/far-red photoreceptor superfamily. *Genome Biol.* **9**, 230 (2008).
6. Rockwell, N.C. & Lagarias, J.C. A brief history of phytochromes. *ChemPhysChem* **11**, 1172–1180 (2010).
7. Li, L., Murphy, J.T. & Lagarias, J.C. Continuous fluorescence assay of phytochrome assembly *in vitro*. *Biochemistry* **34**, 7923–7930 (1995).
8. Giraud, E. *et al.* Bacteriophytochrome controls photosystem synthesis in anoxygenic bacteria. *Nature* **417**, 202–205 (2002).
9. Wagner, J.R. *et al.* Mutational analysis of Deinococcus radiodurans bacteriophytochrome reveals key amino acids necessary for the photochromicity and proton exchange cycle of phytochromes. *J. Biol. Chem.* **283**, 12212–12226 (2008).
10. Shu, X. *et al.* Mammalian expression of infrared fluorescent proteins engineered from a bacterial phytochrome. *Science* **324**, 804–807 (2009).
11. Giraud, E. *et al.* A new type of bacteriophytochrome acts in tandem with a classical bacteriophytochrome to control the antennae synthesis in Rhodopseudomonas palustris. *J. Biol. Chem.* **280**, 32389–32397 (2005).
12. Ulijasz, A.T. *et al.* Characterization of two thermostable cyanobacterial phytochromes reveals global movements in the chromophore-binding domain during photoconversion. *J. Biol. Chem.* **283**, 21251–21266 (2008).
13. Campbell, R.E. *et al.* A monomeric red fluorescent protein. *Proc. Natl. Acad. Sci. USA* **99**, 7877–7882 (2002).
14. Stepanenko, O.V. *et al.* Understanding the role of Arg96 in structure and stability of green fluorescent protein. *Proteins* **73**, 539–551 (2008).
15. Sali, D., Bycroft, M. & Fersht, A.R. Surface electrostatic interactions contribute little of stability of barnase. *J. Mol. Biol.* **220**, 779–788 (1991).
16. Monera, O.D., Kay, C.M. & Hodges, R.S. Protein denaturation with guanidine hydrochloride or urea provides a different estimate of stability depending on the contributions of electrostatic interactions. *Protein Sci.* **3**, 1984–1991 (1994).
17. Muller, L. *et al.* Evolutionary gain of function for the ER membrane protein Sec62 from yeast to humans. *Mol. Biol. Cell* **21**, 691–703 (2010).
18. Scatchard, G. The attraction of proteins for small molecules and ions. *Ann. NY Acad. Sci.* **51**, 660–672 (1949).
19. Strack, R.L. *et al.* A noncytotoxic DsRed variant for whole-cell labeling. *Nat. Methods* **5**, 955–957 (2008).
20. Subramanian, S. & Srienc, F. Quantitative analysis of transient gene expression in mammalian cells using the green fluorescent protein. *J. Biotechnol.* **49**, 137–151 (1996).
21. Warren, L. *et al.* Highly efficient reprogramming to pluripotency and directed differentiation of human cells with synthetic modified mRNA. *Cell Stem Cell* **7**, 618–630 (2010).
22. Strack, R.L. *et al.* A rapidly maturing far-red derivative of DsRed-Express2 for whole-cell labeling. *Biochemistry* **48**, 8279–8281 (2009).
23. Lin, M.Z. *et al.* Autofluorescent proteins with excitation in the optical window for intravital imaging in mammals. *Chem. Biol.* **16**, 1169–1179 (2009).
24. Shcherbo, D. *et al.* Near-infrared fluorescent proteins. *Nat. Methods* **7**, 827–829 (2010).
25. Shcherbo, D. *et al.* Far-red fluorescent tags for protein imaging in living tissues. *Biochem. J.* **418**, 567–574 (2009).
26. Morozova, K.S. *et al.* Far-red fluorescent protein excitable with red lasers for flow cytometry and superresolution STED nanoscopy. *Biophys. J.* **99**, L13–L15 (2010).
27. Kuo, C., Coquoz, O., Troy, T.L., Xu, H. & Rice, B.W. Three-dimensional reconstruction of *in vivo* bioluminescent sources based on multispectral imaging. *J. Biomed. Opt.* **12**, 024007 (2007).
28. Xu, H. & Rice, B.W. *In-vivo* fluorescence imaging with a multivariate curve resolution spectral unmixing technique. *J. Biomed. Opt.* **14**, 064011 (2009).

ONLINE METHODS

Mutagenesis and screening of libraries. A *Rp*BphP2 gene[11] was kindly provided by Eric Giraud. IFP1.4 gene was *de novo* synthesized by GenScript Company, based on the available protein sequence[10]. The DNA sequence was optimized with proprietary OptimumGene algorithm (GenScript), taking into account the codon usage bias (human cells), GC content, CpG dinucleotides content, mRNA secondary structure and other parameters.

The genes encoding a bacteriophytochrome *Rp*BphP2 and an IFP1.4 protein were amplified using PCR as the BglII-EcoRI or PstI-HindIII fragments and inserted into the BglII-EcoRI sites of a pBAD/His-B vector or the PstI and HindIII sites of a pBAD/His-C vector, respectively (Invitrogen). Biliverdin synthesis in bacteria was facilitated by co-transformation with a pPL-BV plasmid, which was obtained after digestion with BamHI and subsequent ligation of the pPL-PCB plasmid[29]. The pPL-PCB plasmid was kindly provided by Andrew Ulijasz and Richard Vierstra.

Site-specific mutagenesis was performed using a QuickChange Mutagenesis Kit (Stratagene). For simultaneous mutagenesis at several positions, including a site-specific saturated mutagenesis (that is, all 20 amino acids were encoded using the mixture of primers), an overlap-extension method was applied[30]. Random mutagenesis was performed with a GeneMorph II Random Mutagenesis Kit (Stratagene), using conditions that resulted in the mutation frequency of up to 16 mutations per 1,000 base pairs. After the mutagenesis, a mixture of mutants was electroporated into the LMG194 host cells (Invitrogen) containing the pPL-BV plasmid.

Typical mutant libraries for FACS screens consisted of 10^7–10^8 independent clones.

LMG194 bacteria were grown overnight in LB medium with an addition of 2% glucose to repress synthesis of both proteins. Next morning, the bacterial cells were centrifuged and resuspended in RM medium with 0.002% arabinose, 0.001 mM IPTG, 100 μM 5-aminolevulinic acid (ALA) and 50 μM $FeCl_3$. The cells were then grown up to 24 h either at 37 °C or 37 °C followed by 25 °C, depending on the experiment.

For FACS screening, protein mutants were expressed in bacteria at 37 °C followed by an overnight incubation at 25 °C. The next morning, bacteria were washed with PBS and then diluted with PBS to an optical density of 0.02 at 600 nm. A MoFlo XDP cell sorter (Beckman Coulter), equipped with the standard Ar, Kr, Ar-Kr mixed-gas lasers (Coherent) and a 592 nm solid-state laser (MPB Communications), was used. Typically, about ten sizes of each library were FACS-sorted, using a 676 nm Kr laser line for excitation and a 700LP nm emission filter for positive selection. The brightest collected near-infrared bacterial cells were rescued in a SOC medium at 37 °C for 1 h and then plated on Petri dishes made of RM/agar supplemented with ampicillin and kanamycin. The next day, the expression of proteins in bacterial colonies on the dishes were induced with 0.002% of arabinose and 0.001 mM of IPTG. The dishes were left for 4–6 h at 37 °C and then incubated at 25 °C overnight.

Fluorescence of the colonies was analyzed the next day using a Leica MZ16F fluorescence stereomicroscope equipped with the 650/45 nm excitation and 690LP nm emission filters (Chroma) and a CCD camera. The 20–30 brightest clones were selected and their DNA was sequenced. A mixture of several selected mutants was then used as a template for the next round of mutagenesis.

Protein characterization *in vitro*. *Rp*BphP2 mutants and IFP1.4 protein with polyhistidine tags were expressed in LMG194 bacterial cells, as described above and then purified using Ni-NTA agarose (Qiagen). The excitation and emission spectra were measured using a FluoroMax-3 spectrofluorometer (Jobin Yvon). For absorbance measurements, a Hitachi U-2000 spectrophotometer was used.

Two different approaches were used to determine extinction coefficients. The first approach was based on a direct measurement of the protein concentrations with a BCA protein assay kit (Pierce), followed by the calculation of extinction coefficients using a Beer-Lambert-Bouguer equation. The second approach, which has been introduced in the original IFP1.4 paper[10], was based on a comparison of absorbance values for the protein at the main peak (692 nm or 694 nm) with the absorbance value at the 391 nm peak assuming the latter to have the extinction coefficient of the free BV, which is 39,900 $M^{-1}cm^{-1}$. For determination of quantum yield, fluorescence signal of iRFP was compared to that of the equally absorbing IFP1.4 and Nile Blue dye (quantum yield is 0.27 in an acidic ethanol[31]).

pH titrations were done using a series of buffers (100 mM sodium acetate, 300 mM NaCl for pH 2.5–5.0 and 100 mM NaH_2PO_4, 300 mM NaCl for pH 4.5–9.0).

To study protein maturation, LMG194 bacterial cells were grown at 37 °C overnight in a LB medium supplemented with ampicillin, kanamycin and 2% of glucose. The next morning, the cells were centrifuged, resuspended and cultured in RM medium with 0.002% arabinose, 0.001 mM IPTG, 100 μM ALA and 50 μM $FeCl_3$ for 1 h. Then, the cells were washed and cultured in RM medium supplemented with 0.001 mM IPTG, 100 μM ALA and 50 μM $FeCl_3$ (no arabinose was added this time) at 37 °C. Fluorescence intensity of the cell suspension was measured every hour initially and after longer time periods later.

Covalent BV attachment to the proteins was tested as it has been described[32].

Mammalian plasmids and cell culture. A pShuttle-CMV vector (Stratagene) was used to construct plasmids for mammalian expression of both iRFP and IFP1.4 proteins. The fluorescent protein genes were PCR-amplified and inserted into the BglII and SalI sites of the vector, thus generating pShuttle-CMV-iRFP and pShuttle-CMV-IFP1.4 plasmids.

HEK293 and HeLa cell lines were grown in DMEM containing 10% FBS, penicillin-streptomycin and 2 mM glutamine (Invitrogen). Cells were cultured in 35 mm glass bottom culture dishes with no. 1 cover glasses (MatTek). Plasmid transfections were performed using an Effectene reagent (Qiagen) according to the manufacturer's protocol.

For adenoviral infection, HeLa cells were grown in 60 mm Petri dishes until ~80% confluence and then infected with 3×10^7 PFU per dish.

Characterization in mammalian cells. For FACS analysis of HeLa cells co-transfected with EGFP and near-infrared fluorescent proteins, 488 nm Ar and 676 nm Kr laser lines and the respective 530/40 nm and 700LP nm emission filters were used. To quantify cell fluorescence, a mean fluorescent intensity of the double-positive population in the near-infrared channel was divided by a mean fluorescence intensity of the same population in the green channel, thus normalizing the near-infrared signal to the transfection efficiency.

Imaging of HeLa and HEK293 cells was done 48 h after the transfection. Cells were imaged using an Olympus IX81 inverted epifluorescence microscope equipped with 200 W metal halide arc lamp (Prior), a 100× 1.4 NA oil immersion objective lens (UPlanSApo, Olympus) and standard Cy5.5 filter set (665/45 nm exciter and 725/50 nm emitter) (Chroma).

Photobleaching measurements of cytoplasmically expressed near-infrared fluorescent proteins in live HeLa cells were performed similarly to the purified proteins with the 100× objective substituted with a 60× 1.35 NA oil immersion objective lens (UPlanSApo, Olympus). Normalization of the curves was made the same way as for the purified proteins.

For the protein degradation assay, HEK293 cells transfected with near-infrared fluorescent proteins were treated with 1 mM of puromycin 48 h after transfection. To achieve a brighter fluorescence signal, cells were kept with 25 μM of BV during the whole experimental course, starting 2 h before the addition of the puromycin.

To study BV binding and BV influence on protein stability, HeLa cells were harvested 2 d after adenoviral infection and lysed by three freezing-thawing cycles. The lysates were clarified by centrifugation and the total fluorescence was measured using the FluoroMax-3 spectrofluorometer (Jobin Yvon).

Construction of adenoviral vectors. The adenovirus serotype V–based particles containing the iRFP or IFP1.4 genes were created using an AdEasy XL Adenoviral Vector System (Stratagene) according to the manufacturer's recommendations and then purified using a cesium chloride gradient centrifugation, as described[33]. The viral titers were assessed by an Adeno-X Rapid Titer Kit (Clontech). Construction of adenoviruses encoding the GFP/S65T variant was described earlier[34].

***In vivo* imaging.** Albino C57BL/6 mice (female 6–8 weeks old, B6(Cg)-*Tyr*$^{c\text{-}2J}$/J, Jackson Laboratory) were intravenously injected with 2×10^9 infectious units of an adenovirus. Belly fur was removed using a depilatory cream and the

doi:10.1038/nbt.1918

mice imaging was performed with an IVIS Spectrum instrument (Caliper LifeSciences) in epifluorescence mode equipped with 675/30 nm and 720/20 nm filters for excitation and emission, respectively, starting the second day after an infection. 250 nmol of BV were intravenously injected on day 5 after infection and the mice imaging started 1 h later. Quantitative measurements of fluorescence signal were made with a Living Image Software 4.0 (Caliper LifeSciences). For *ex vivo* liver imaging, mice were euthanized and livers were dissected 1 h after mice were injected with 250 nmol of BV. The isolated livers or spleens were imaged with the IVIS Spectrum instrument. All animal experiments were performed in a facility approved by the Association for Assessment and Accreditation of Laboratory Animal Care using protocols approved by the Albert Einstein College of Medicine Animal Usage Committee.

Protein imaging in phantom mouse. Bacterial plasmids encoding several far-red GFP-like fluorescent proteins were kindly provided by Benjamin Glick and Dmitry Chudakov and Konstantin Lukyanov. The recombinant GFP-like fluorescent proteins were expressed in the LMG194 bacterial cells and then purified using the Ni-NTA agarose (Qiagen). The purified fluorescent proteins were diluted to the equal concentrations of 16 μM, calculated based on the extinction coefficients at the chromophore absorbance maxima. The 5 μl volume of each fluorescent protein was placed 15 mm deep inside into one of two available bores in a XFM-2 phantom mouse (Caliper LifeSciences). The bores were located at 7.0 mm and 18.1 mm distance from the imaging surface. Images were taken in 23 different combinations of the far-red and near-infrared excitation and emission channels using an epifluorescence mode of the IVIS Spectrum instrument. A signal-to-background ratio was calculated for each wavelength combination for each fluorescent protein, using the phantom mouse without protein sample inside as a background reference. All quantitative measurements of fluorescence signal were performed using the Living Image Software 4.0.

29. Gambetta, G.A. & Lagarias, J.C. Genetic engineering of phytochrome biosynthesis in bacteria. *Proc. Natl. Acad. Sci. USA* **98**, 10566–10571 (2001).
30. Ho, S.N., Hunt, H.D., Horton, R.M., Pullen, J.K. & Pease, L.R. Site-directed mutagenesis by overlap extension using the polymerase chain reaction. *Gene* **77**, 51–59 (1989).
31. Drexhage, R.S.K.H. Fluorescence quantum yield of oxazine and carbazine laser dyes. *J. Lumin.* **24–25**, 709–712 (1981).
32. Lamparter, T. *et al.* Biliverdin binds covalently to agrobacterium phytochrome Agp1 via its ring A vinyl side chain. *J. Biol. Chem.* **278**, 33786–33792 (2003).
33. Luo, J. *et al.* A protocol for rapid generation of recombinant adenoviruses using the AdEasy system. *Nat. Protoc.* **2**, 1236–1247 (2007).
34. Cohen, D., Brennwald, P.J., Rodriguez-Boulan, E. & Musch, A. Mammalian PAR-1 determines epithelial lumen polarity by organizing the microtubule cytoskeleton. *J. Cell Biol.* **164**, 717–727 (2004).